J|A|C|S
ARTICLES
Published on Web 04/08/2006

# Solution Structures of Human LL-37 Fragments and NMR-Based Identification of a Minimal Membrane-Targeting Antimicrobial and Anticancer Region

Xia Li,[†] Yifeng Li,[†,‡] Huiyun Han,[§] Donald W. Miller,[§] and Guangshun Wang*[,†,‡,§]

*Contribution from the Eppley Institute for Research in Cancer and Allied Diseases, Department of Pathology and Microbiology, and College of Pharmacy, University of Nebraska Medical Center, 986805 Nebraska Medical Center, Omaha, Nebraska 68198-6805*

Received December 22, 2005; E-mail: gwang@unmc.edu

***Abstract:*** To understand the structure and activity relationship of human LL-37, a series of peptide fragments was designed. The N-terminal fragment, LL-37(1−12), was not active, while the C-terminal fragment, LL-37(13−37), killed *Escherichia coli*, as well as drug-sensitive and drug-resistant cancer cells. A 13-residue core antibacterial and anticancer peptide, corresponding to residues 17−29 of LL-37, was identified based on total correlated spectroscopy by trimming nonessential regions (TOCSY-trim). Because LL-37 acts on bacterial membranes, three-dimensional structures of its fragments were determined in micelles by NMR, including structural refinement by natural abundance $^{15}N$ and $^{13}C$ chemical shifts. Aromatic−aromatic interactions in the N-terminal fragment were proposed to be essential for LL-37 aggregation. The LL-37 core peptide adopts a similar structure in the micelles of SDS or dioctanoyl phosphatidylglycerol. This structure is retained in the C-terminal fragment LL-37(13−37) and very likely in intact LL-37 based on peptide-aided signal assignments. The higher antibacterial activity of the LL-37 core peptide than aurein 1.2 was attributed to additional cationic residues. To achieve selective membrane targeting, D-amino acids were incorporated into LL-37(17−32). While the D-peptide showed similar antibacterial activity to the L-diastereomer, it lost toxicity to human cells. Structural analysis revealed hydrophobic defects in the new amphipathic structure of the D-peptide, leading to a much shorter retention time on a reversed-phase HPLC column. It is proposed that hydrophobic defects as a result of incoherent hydrophobic packing provide a structural basis for the improvement in cell selectivity of the LL-37 fragment.

## Introduction

The search for novel antimicrobial agents is intensifying, in response to both the threat of microbial pathogens in bioterrorism and the increasing development of drug resistance to current antibiotic therapeutics. Antimicrobial peptides are essential host defense molecules found in a wide variety of species and are promising antibacterial therapeutic candidates.[1,2] Several hundreds of antimicrobial peptides have been identified in a variety of life forms ranging from bacteria, fungi, plants, amphibians, to mammals, including humans.[3−5] In mammals, cathelicidins and defensins are the two major types of host defense peptides.[6] Defensins usually contain three pairs of disulfide bonds that stabilize the protein fold. Cathelicidins, however, are rather variable in both sequence and structure, although their precursor proteins share a common N-terminal "cathelin" domain. Cathelicidins are classified into three groups. The first group of cathelicidin peptides contains 12−18 residues with beta-hairpin structures stabilized by one or two disulfide bonds. This group also includes a 13-residue linear peptide with a high content of tryptophans. The second group contains 23−37 residues and has the potential to form a helical structure. The peptides in the third group such as PR-39 are rich in prolines with 39−80 residues (for a review, see ref 6).

LL-37 is the only human cathelicidin identified to date. It has been detected in a variety of cells such as B cells, monocytes, mast cells, and immature neutrophils.[7−9] Several lines of evidence support the significance of this human peptide in host defense. First, the precursor gene of LL-37 (hCAP-18) is up-regulated in skin in response to cutaneous infection as well as in inflammatory skin disorders such as psoriasis.[10,11] Second, LL-37 deficiency in neutrophils correlates with the

[†] Eppley Institute.
[‡] Department of Pathology and Microbiology.
[§] College of Pharmacy.

(1) Zasloff, M. *Nature* **2002**, *415*, 389−395.
(2) Mcphee, J. B.; Hancock, R. E. W. *J. Pept. Sci.* **2005**, *11*, 677−687.
(3) Mygind, P. H.; et al. *Nature* **2005**, *437*, 975−80.
(4) Brahmachary, M.; Krishnan, S. P.; Koh, J. L.; Khan, A. M.; Seah, S. H.; Tan, T. W.; Brusic, V.; Bajic, V. B. *Nucleic Acids Res.* **2004**, *32*, D586−589.
(5) Wang, Z.; Wang, G. *Nucleic Acids Res.* **2004**, *32*, D590−D592.
(6) Zanetti, M. *J. Leukoc. Biol.* **2004**, *75*, 39−48.
(7) Sorensen, O.; Arnljots, K.; Cowland, J. B.; Bainton, D. F.; Borregaard, N. *Blood* **1997**, *90*, 2796−2803.
(8) Agerberth, B.; Charo, J.; Werr, J.; Olsson, B.; Idali, F.; Lindbom, L.; Kiessling, R.; Jornvall, H.; Wigzell, H.; Gudmundsson, G. H. *Blood* **2000**, 96, 3086−3093.
(9) Di Nardo, A.; Vitiello, A.; Gallo, R. L. *J. Immunol.* **2003**, 170, 2274−2278.


**10.1021/ja0584875 CCC: $33.50** 

occurrence of chronic periodontal diseases in patients with morbus Kostmann.[12] Third, gene knockout of the CRAMP cathelicidin in mice increases their susceptibility to skin infection.[13] Fourth, expression of additional cathelicidins by gene transfer protects against skin infection by bacteria.[14] In addition to its antibacterial effects, human LL-37 appears to play an important role in angiogenesis, chemotaxis,[6] and signal transduction as well.[15,16] Structural biology of LL-37 should provide insight into the multiple functions of this important human host defense peptide.

According to previous circular dichroism (CD) studies, LL-37 forms helical structures upon increasing peptide concentration, anions, pH, detergents, and lipids.[17,18] The helicity of the peptide was found to correlate with antibacterial activity. Recent solid-state NMR, differential scanning calorimetry, and biochemical analysis substantiated the interactions of LL-37 with lipid bilayers.[17−20] However, no three-dimensional structure has been reported for LL-37. To provide structural insight into the multiple functions of this important human defense peptide, we present, in this article, the solution structures of the fragments of LL-37 in complex with detergent micelles, which mimic bacterial membranes.[21,22] The quality of micelle-bound structures was improved by utilizing natural abundance chemical shifts.[23] During our study, Gallo and colleagues reported that, after secretion onto the skin surface, human LL-37 in sweat could be cleaved (e.g., after residue F6 or R7) into more active antibacterial and antifungal fragments with a reduced toxicity to erythrocytes.[24] Further, these contracted forms of LL-37 lost their capability of stimulating a host response possessed by the full-length peptide. Therefore, their finding endowed biological relevance to our structural studies of LL-37 fragments. In addition, we have identified the shortest antibacterial fragment within LL-37 based on TOCSY-trim, a technique that effectively trims nonessential membrane-targeting peptide regions based on the TOCSY patterns of side-chain resonances. Finally, it is feasible to detoxify LL-37 fragments by introducing D-amino acids. The structural basis for improving cell selectivity was elucidated. We propose that D-amino acid generated hydrophobic defects, because of the incoherent packing of hydrophobic clusters, disrupt the binding of the D-peptide to human cells.

## Methods

**Antibacterial Assays.** The antibacterial activity of the LL-37 peptides and its analogues was analyzed using the standard approach of microdilution.[23,25] In brief, a small culture of wild type *E. coli* K12 (gift from Dr. Alan Peterkofsky, NIH) was grown overnight. A fresh culture was inoculated with a small aliquot of the overnight culture and incubated at 37 °C until the optical density reached the mid-logarithmic stage. The culture (90 $\mu$L each) was then diluted to an $A_{600}$ of 0.001 and partitioned into a 96-well plate with $\sim 10^6$ cells per well. The cells were then treated with 10 $\mu$L of the peptide at a series of levels (5 to 320 $\mu$M), allowing the minimum inhibitory concentration (MIC) measurement for each. Each peptide assay was repeated 3 times. The plate was then further incubated at 37 °C overnight ($\sim$16 h) and read on an Ultra Microplate Reader at 620 nm (Bio-TEK Instruments).

**Anticancer Assays.** Cytotoxicity studies were performed using the colorimetric MTT assays for assessing cell viability.[26,27] Three cell lines were used, including drug-resistant KBv, drug-sensitive KB, and the nontransformed human brain microvessel endothelial cells (HBMEC). In brief, the cells were seeded onto 96-well plates at a density of 5000 cells per well. The cells were exposed to various concentrations (5−320 $\mu$M) of LL-37 peptides (triplicate assays for each) 24 h after seeding. After 68 h of exposure, the peptide solution was replaced with fresh media and followed by cytotoxicity analysis using the MTT assay.

The MTT assay was performed by incubating the cells with 5 mg/mL of 3-[4,5-dimethylthiazol-2-yl]-2,5-dephenyltetrazolium bromide (MTT) for 2 h at 37 °C. The cells were then solubilized in a 50:50 mixture of dimethyl formamide (DMF) and $H_2O$ containing 20% SDS (pH 4.7). The plates were read after overnight incubation. Viability is directly proportional to the amount of metabolic conversion of MTT to formazin in the mitochondria of living cells and is assessed by measuring the absorbance at 550 nm using a Microkinetics Reader (Fisher Biotech). Viability is expressed as a percent of control cells receiving only culture media without any peptides. The data from the cytotoxicity studies were plotted using Microsoft Excel, and the $LC_{50}$ (concentration resulting in 50% reduction in cell viability) and standard deviations were determined for each peptide.

**Analytical Reversed-Phase HPLC.** The retention time of the peptide was measured on an ISCO HPLC system equipped with a Vydac C18 reversed-phase column (250 × 4.6 mm) at an ambient temperature of $\sim$25 °C. The peptide was eluted with a linear gradient of acetonitrile (containing 0.1% TFA) from 5% to 95% at a flow rate of 1 mL/min. Peptides were detected by UV absorbance at 215 nm.

**NMR Spectroscopy.** All peptides were synthesized and purified (>95% purity) by Genemed Synthesis, Inc. (San Francisco). For NMR measurements, the peptide concentration was typically $\sim$2 mM in 0.6 mL of aqueous solution of 90% $H_2O$ and 10% $D_2O$ at pH 5.4. The pH of each sample was adjusted by using microliter aliquots of HCl or NaOH solution and measured directly in the 5-mm NMR tube with a micro-pH electrode (Wilmad-Labglass). The peptide/SDS molar ratio was 1:40, and the peptide/dioctanoyl phosphatidylglycerol (D8PG, Avanti Lipids) ratio was 1:5. These ratios were found to be sufficient for the peptides to adopt micelle-bound conformations.

All data were recorded on a four-channel Varian INOVA 600 MHz NMR spectrometer equipped with a triple-resonance cryoprobe with a *z*-axis gradient. A set of 2D NMR spectra was collected for each peptide using States-TPPI at 25 °C. In addition, data were also collected at 15 °C for the N-terminal fragment and at 35 °C for the C-terminal fragment of LL-37. NOESY[28] spectra were acquired at a mixing time of 100 ms for peptide/micelle complexes. TOCSY[29,30] experiments were performed


(10) Dorschner, R. A.; Pestonjamasp, V. K.; Tamakuwala, S.; Ohtake, T.; Rudisill, J.; Nizet, V.; Agerberth, B.; Gudmundsson, G. H.; Gallo, R. L. *J. Invest. Dermatol*. **2001**, *117*, 91−97.
(11) Frohm, M.; Agerberth, B.; Ahangari, G.; Stahle-Backdahl, M.; Liden, S.; Wigzell, H.; Gudmundsson, G. H. *J. Biol. Chem.* **1997**, *272*, 15258−15263.
(12) Putsep, K.; Carlsson, G.; Boman, H. G.; Andersson, M. *Lancet* **2002**, *360*, 1144−1149.
(13) Nizet, V.; Ohtake, T.; Lauth, X.; Trowbridge, J.; Rudisill, J.; Dorschner, R. A.; Pestonjamasp, V.; Piraino, J.; Huttner, K.; Gallo, R. L. *Nature* **2001**, *414*, 454−457.
(14) Lee, P. H.; Ohtake, T.; Zaiou, M.; Murakami, M.; Rudisill, J. A.; Lin, K. H.; Gallo, R. L. *Proc. Natl. Acad. Sci. U.S.A.* **2005**, *102*, 3750−3755.
(15) Bowdish, D. M. E.; Davidson, D. J.; Speert, D. P.; Hancock, R. E. W. *J. Immunol.* **2004**, *172*, 3758−3765.
(16) Tjabringa, G. S.; Aarbiou, J.; Ninaber, D. K.; Drijfhout, J. W.; Sorensen, O. E.; Borregaard, N.; Rabe, K. F.; Hiemstra, P. S. *J. Immunol*. **2003**, *171*, 6690−6696.
(17) Johansson, J.; Gudmundsson, G. H.; Rottenberg, M. E.; Berndt, K. D.; Agerberth, B. *J Biol. Chem.* **1998**, *273*, 3718−24.
(18) Oren, Z.; Lerman, J. C.; Gudmundsson, G. H.; Agerberth, B.; Shai, Y. *Biochem. J.* **1999**, *341*, 501−13.
(19) Henzler-Wildman, K. A.; Martinez, G. V.; Brown, M. F.; Ramamoorthy, A. *Biochemistry* **2004**, *43*, 8459−69.
(20) Henzler-Wildman, K. A.; Lee, D. K.; Ramamoorthy, A. *Biochemistry* **2003**, *42*, 6545−58.
(21) Henry, G. D.; Sykes, B. D. *Methods Enzymol.* **1994**, *239*, 515−535.
(22) Opella, S. J.; Marassi, F. M. *Chem. Rev.* **2004**, *104*, 3587−3606.
(23) Wang, G.; Li, Y.; Li, X. *J. Biol. Chem.* **2005**, *280*, 5803−5811.
(24) Murakami, M.; Lopez-Garcia, B.; Braff, M.; Dorschner, R. A.; Gallo, R. L. *J Immunol*. **2004**, *172*, 3070−3077.
(25) Yu, K.; Park, K.; Kang, S.-W.; Shin, S. Y.; Hahm, K.-S.; Kim, Y. *J. Pept. Res.* **2002**, *60*, 1−9.
(26) Mark, K. S.; Miller, D. W. *Life Sci.* **1999**, *64*, 1941−1953.
(27) Hansen, M. B.; Nielsen, S. E.; Berg, K. *J. Immunol. Methods* **1989**, *119*, 203−210.
(28) Jeener, J.; Meier, B. H.; Bachmann, P.; Ernst, R. R. *J. Chem. Phys.* **1979**, *71*, 4546−4553.
(29) Bax, A.; Davis, D. G. *J. Magn. Reson.* **1985**, *65*, 355−360.

with a mixing time of 75 ms using a clean MLEV-17 pulse sequence. Two-dimensional homonuclear NMR spectra were collected with 512 increments (16−32 scans each) in t1 and 2K complex points in t2 time domains using a spectral width of 8510.6 Hz in both dimensions with the $^1$H carrier on water. In NOESY and TOCSY experiments, the water signal was suppressed by presaturation or WATERGATE;[31] for DQF-COSY[32] experiments, water was suppressed by low power presaturation during relaxation delay.

Two 2D heteronuclear NMR spectra were recorded for each peptide at natural abundance using a gradient-enhanced version of HSQC experiments.[33] For the $^1$H and $^{15}$N correlation, 30 increments (128 scans) were collected in the $^{15}$N dimension at a spectral width of 2200 Hz. For the $^1$H and $^{13}$C correlation, 80 increments (256 scans) were collected in the $^{13}$C dimension at a spectral width of 12 000 Hz. The data size in the proton dimension was 512 complex points. In these correlated spectra, the $^1$H, $^{15}$N, and $^{13}$C carriers were set at 4.77, 118.27, and 36.37 ppm, respectively.

All NMR data were processed on a Silicon Graphics Octane workstation (SGI) using the NMRPipe software.[34] Time domain data were apodized by a 63° shifted squared sine-bell window function in both dimensions, zero-filled prior to Fourier transformation to yield a 2K × 1K data matrix. To avoid the interaction of anionic 2,2-dimethylsilapentane-5-sulfonate sodium salt (DSS) with cationic peptides,[35,36] the proton chemical shifts of the peptide were referenced to the water signal, which in turn was referenced to the methyl signal of internal DSS at 0.00 ppm. $^{15}$N and $^{13}$C chemical shifts were referenced based on the relative frequency ratios recommended by IUPAC.[37]

NMR data were analyzed using NMRDraw in the NMRPipe suite[34] as well as PIPP.[38] The peptide proton signals were assigned using the standard procedure[39] based on 2D TOCSY, DQF-COSY, and NOESY spectra. The $^{13}$C$\alpha$, $^{13}$C$\beta$, and $^{15}$N resonances for each peptide were assigned on the basis of the proton chemical shift assignments achieved above.[40]

**Structure Calculations.** Three-dimensional structures of the peptides bound to deuterated SDS (Cambridge Isotope Laboratory) micelles at pH 5.4 and 25 °C were calculated based on both distance and angle restraints by using the simulated annealing protocol in Xplor-NIH.[41] The structure for the N-terminal fragment LL-37(1−12) was calculated using the 15 °C data due to a better NOESY spectrum. The distance restraints were obtained by classifying the NOE cross-peak volumes into strong (1.8−2.8 Å), medium (1.8−3.8 Å), weak (1.8−5.0 Å), and very weak (1.8−6.0 Å) ranges. The distance was calibrated on the basis of the typical NOE patterns in an α helix.[39] Peptide backbone restraints were obtained from the TALOS[42] analysis of a set of heteronuclear chemical shifts, including $^1$H$\alpha$, $^{13}$C$\alpha$, $^{13}$C$\beta$, and $^{15}$N. A broader range (up to ±20°) than predicted was allowed for each angle in the structural calculations. In each case, a covalent peptide structure with random $\phi$, $\psi$, and $\chi$ angles, but trans planar peptide bonds, was used as a starting structure. In total, 100 structures were calculated. An ensemble of 20 structures with the lowest total energy was chosen for structural analysis. This final ensemble of accepted structures satisfies the following criteria: no NOE violations greater than 0.5 Å, root-mean-square deviation (rmsd) for bond deviations from ideality less than 0.01 Å, and rmsd for angle deviations from ideality less than 5°.

The coordinates of the LL-37 core peptide and the N- and C-terminal fragments of LL-37 in SDS micelles have been deposited with the Protein Data Bank (PDB entries: 2FBS, 2FBU, and 2FCG).

***Table 1.*** Name, Sequences, and HPLC Retention Times of Peptides

| peptide | sequence | $t^{RP}$ (min)[a] |
|---|---|---|
| LL-37(1−12) | LLGDFFRKSKEK | 26.6 |
| LL-37(13−37) | IGKEFKRIVQRIKDFLRNLVPRTES | 39.8 |
| LL-37(17−32)[b] | FKRIVQRIKDFLRNLV | 42.0 |
| LL-37(17−29) | FKRIVQRIKDFLR | 37.2 |
| LL-37(1−4,17−27) | LLGD FKRIVQRIKDF | 32.8 |
| dLL-37(17−32)[c] | FKR**I**VQR**I**KDF**L**RNLV | 29.8 |
| aurein 1.2 | GLF$\bar{D}$IIKK$\bar{I}$AES$\bar{F}$ | 42.0 |
| anchor[d] | GLFDKLKSLVSDDKK | 29.5 |

[a] Retention time of the peptide (in minutes) on a reversed-phase HPLC column as a measure of hydrophobicity.[61−62] [b] Several peptides, including LL-37(17−29), LL-37(17−32), dLL-37(17−32), and LL-37(1−4,17−27), were amidated at the C-terminus to improve the stability of the peptides. [c] Residues I20, I24, and L28 of this peptide are D-amino acids (bold and underlined). [d] The bacterial membrane anchor of glucose-specific enzyme IIA$^{Glc}$ of *E. coli*.[63]

## Results and Discussion

**Identification of a Core Antibacterial and Anticancer Peptide from LL-37 by TOCSY-Trim and Activity Assays.** Human LL-37 is a 37-residue peptide with a pair of leucines (LL) at the N-terminus. Its primary sequence is LLGDFFRKSKEKIGKEFKRIVQRIKDFLRNLVPRTES.[43] Previous antibacterial assays using *Escherichia coli* D21 revealed MIC values in the range 5−25 $\mu$M.[17,18] Using the wild type *E. coli* K12 strain, we found an MIC of 40 $\mu$M for LL-37.[44] To narrow down the antibacterial region in LL-37, a series of peptides was designed (Table 1). Initially, LL-37 was cut into halves. The "cutting point" was chosen at the end of a string of six hydrophilic residues (underlined in the above sequence) and in the vicinity of G14 of the peptide. Hence, the N-terminal fragment corresponds to residues 1−12 of LL-37 (referred to as LL-37(1−12)), while the C-terminal fragment corresponds to residues 13−37 (referred to as LL-37(13−37)). Antibacterial and anticancer assays showed that the N-terminal fragment was not active, while the C-terminal fragment had toxic effects on drug-resistant KBv and drug-sensitive KB cancer cells as well as *E. coli* (Table 2). Localization of antibacterial and antineoplastic activity at the C-terminal region of LL-37 is consistent with previous studies.[17,18,24,45−47]

In light of these observations, a third peptide was created based on the TOCSY spectrum of LL-37(13−37) by trimming off disordered regions (Figure 1A). In the TOCSY spectrum, the structured portion of a peptide, due to association with micelle, gives very weak or no cross-peaks from the backbone amide protons to side chains, whereas those disordered peptide regions or weakly micelle-binding regions display intense cross-peaks.[36,48,49] In Figure 1A, strong TOCSY patterns for residues 30−32 and 34−37 were labeled. Further, two or more sets of intense cross-peaks were observed for residue G14, E16, T35,

(30) Griesinger, C.; Otting, G.; Wüthrich, K.; Ernst, R. R. *J. Am. Chem. Soc.* **1988**, *110*, 7870−7872.
(31) Piotto, M.; Saudek, V.; Sklenar, V. *J. Biomol. NMR* **1992**, *2*, 661−665.
(32) Rance, M.; Sørensen, O. W.; Bodenhausen, G.; Wagner, G.; Enrst, R. R.; Wüthrich, K. *Biochem. Biophys. Res. Commun.* **1983**, *117*, 479−485.
(33) Kay, L. E.; Keifer, P. A.; Saarinen, T. *J. Am. Chem. Soc.* **1992**, *114*, 10663−10665.
(34) Delaglio, F.; Grzesiek, S.; Vuister, G. W.; Zhu, G.; Pfeifer, J.; Bax, A. *J. Biomol. NMR* **1995**, *6*, 277−293.
(35) Keifer, P. A.; Peterkofsky, A.; Wang, G. *Anal. Biochem.* **2004**, *331*, 33−39.
(36) Wang, G.; Keifer, P. A.; Peterkofsky, A. *Protein Sci.* **2003**, *12*, 1087−1096.
(37) Markley, J. L.; Bax, A.; Arata, Y.; Hilbers, C. W.; Kaptein, R.; Sykes, B. D.; Wright, P. E.; Wüthrich, K. *J. Biomol. NMR* **1998**, *12*, 1−23.
(38) Garrett, D. S.; Powers, R.; Gronenborn, A. M.; Clore, G. M. *J. Magn. Reson.* **1991**, *95*, 214−220.
(39) Wüthrich, K. *NMR of Proteins and Nucleic Acids*; Wiley: New York, 1986.
(40) Wang, G. *Curr. Org. Chem.* **2006**, *10*, 569−581.
(41) Schwieters, C. D.; Kuszewski, J.; Tjandra, N.; Clore, G. M. *J. Magn. Reson.* **2003**, *160*, 65−73.
(42) Cornilescu, G.; Delaglio, F.; Bax, A. *J. Biomol. NMR* **1999**, *13*, 289−302.
(43) Gudmundsson, G. H.; Agerberth, B.; Odeberg, J.; Bergman, T.; Olsson, B.; Salcedo, R. *Eur. J. Biochem.* **1996**, *238*, 325−332.
(44) Li, Y.; Li, X.; Wang, G. *Protein Expression Purif.*, in press.

***Table 2.*** Antibacterial and Anticancer Activity of LL-37 Fragments

| peptide | *E. coli* MIC[a] ($\mu$M) | KBv $LC_{50}$[b] ($\mu$M) | KB $LC_{50}$ ($\mu$M) | HBMEC $LC_{50}$ ($\mu$M) |
|---|---|---|---|---|
| LL-37(1−12) | NE[c] | NE | NE | NE |
| LL-37(13−37) | 80 | 39 ± 0 | 40 ± 0 | 38 ± 3 |
| LL-37(17−32) | 20 | 30 ± 0 | 30 ± 1 | 25 ± 1 |
| LL-37(17−29) | 40 | 60 ± 0 | 57 ± 3 | 55 ± 2 |
| LL-37(1−4,17−27) | 250 | NE | NE | NE |
| dLL-37(17−32)[d] | 40 | NE | NE | NE |

[a] Minimum inhibitory concentration measured as described in Methods. The peptides were quantified using the method of Waddell.[66] In this method, the peptide concentration (in mg/mL) is calculated by using the difference in UV absorbance at 215 and 225 nm multiplied by 0.144. [b] The peptide concentration that kills 50% of the cells. [c] "NE" stands for no toxic effect. [d] This D-peptide analogue contains an additional glycine at the N-terminus. It has identical antibacterial activity to that of its corresponding L-diastereomer (i.e., consisting of all L-amino acids).

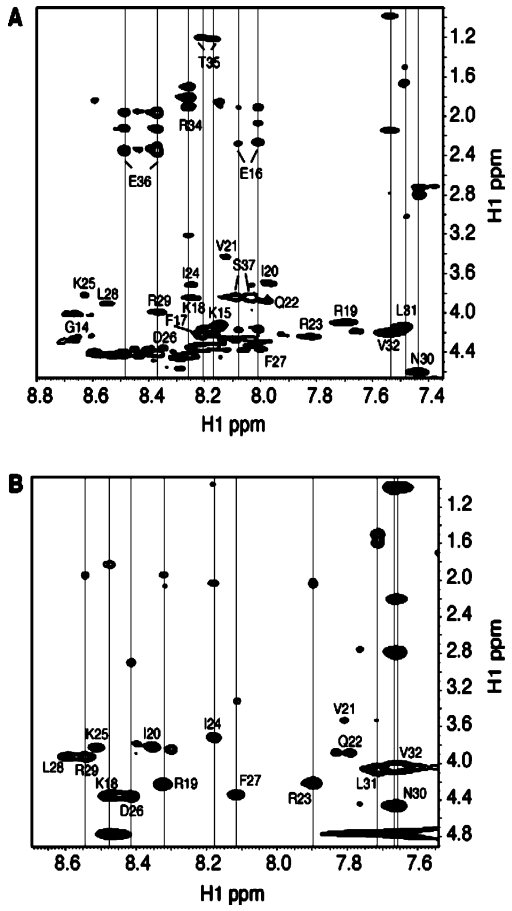


***Figure 1.*** TOCSY spectra of LL-37(13−37) (A) and LL-37(17−32) (B) in SDS micelles. TOCSY-trim is a technique that identifies disordered or weakly micelle-binding peptide regions based on strong cross-peaks (e.g., residues 34−37 in panel A and 30−32 in panel B). Trimming such regions had small effects on the antibacterial and anticancer activity of the peptide (Table 2).

E36, and S37, indicating multiple conformations. The cross-peaks for other residues of the peptide were barely visible. As a consequence, a third peptide, LL-37(17−32), was obtained by removing nonessential micelle-binding residues 13−16 as well as 33−37 from LL-37(13−37). Antibacterial and anticancer assays found that LL-37(17−32) was more active than LL-37-(13−37).

The peptide was further shortened based on the TOCSY spectrum of LL-37(17−32) in SDS micelles (Figure 1B). Clearly, side-chain peak intensities for residues N30, L31, and V32 were much stronger than those for residues 17−29. Note that N30, L31, and V32 also gave strong TOCSY relays in Figure 1A, indicating that the flexibility of these residues was inherent and not a result of peptide truncation. Therefore, residues 30−32 were also deleted, leading to a fourth peptide LL-37(17−29) of only 13 residues. Compared to LL-37(17−32), both the antibacterial and anticancer activities of LL-37-(17−29) were reduced (Table 2). These results suggest that residues N30−V32 play a role in determining the cytotoxic effects of LL-37. In the two cancer cell lines and one normal human cell line we tested, these LL-37 fragments showed no cell selectivity, consistent with the previous observations that LL-37 is toxic to human cells.[17,18]

To design a miniature version of LL-37, we removed L28R29 from LL-37(17−29) and added residues 1−4 to the N-terminus. The resultant peptide, LL-37(1−4,17−27), nevertheless, is no longer active. These particular studies emphasize the importance of residues L28R29 for both antimicrobial and anticancer cytotoxic effects of the peptide.

Other laboratories also found or designed a variety of LL-37 fragments using different strategies. Using V8 proteinase hydrolysis, Sieprawska-Lupa et al. found LL-37(17−37), which is as active as the intact molecule against *Staphylococcus aureus*.[45] Likewise, Nagaoka et al. improved the lipopolysaccharide-neutralizing ability of LL-37(15−32) by site-directed mutagenesis.[46] Using a synthetic peptide library of LL-37, Gallo and colleagues[47] found LL-37(11−30) with a broad spectrum of antimicrobial activity. A recent paper systematically scanned LL-37 by synthesizing numerous 22mers.[50] LL-37(14−36) was chosen and further modified by site-directed mutagenesis. Interestingly, all these active peptides contain the essential segment corresponding to residues 17−29 of LL-37, which we found by TOCSY-trim (Figure 1). Because LL-37(17−29) is the shortest antimicrobial and anticancer peptide identified to date,[17,18,23,40−42] we may refer to this segment as the LL-37 core peptide.

**Structure of the LL-37 Core Peptide.** To further understand the antibacterial activity of the LL-37 core peptide, we have determined its 3D structure in detergent micelles by the established 2D NMR approach.[39] Because the major anionic lipids in bacteria are phosphatidylglycerols (PGs), we have demonstrated the use of short chain PGs for structural determination of antimicrobial peptides by liquid-state NMR.[35,36,52] Thus, the NOESY spectra for the LL-37 core peptide were collected in D8PG micelles. As a comparison, the Hα chemical

(45) Sieprawska-Lupa, M.; Mydel, P.; Krawczyk, K.; Wojcik, K.; Puklo, M.; Lupa, B.; Suder, P.; Silberring, J.; Reed, M.; Pohl, J.; Shafer, W.; McAleese, F.; Foster, T.; Travis, J.; Potempa, J. *Antimicrob. Agents Chemother*. **2004**, *48*, 4673−4679.
(46) Nagaoka, I.; Hirota, S.; Niyonsaba, F.; Hirata, M.; Adachi, Y.; Tamura, H.; Tanaka, S.; Heumann, D. *Clin. Diagn. Lab Immunol*. **2002**, *9*, 972−982.
(47) Braff, M. H.; Hawkins, M. A.; Di Nardo, A.; Lopez-Garcia, B.; Howell, M. D.; Wong, C.; Lin, K.; Streib, J. E.; Dorschner, R.; Leung, D. Y.; Gallo, R. L. *J Immunol*. **2005**, *174*, 4271−4278.
(48) Wang, G.; Pierens, G. K.; Treleaven, W. D.; Sparrow, J. T.; Cushley, R. J. *Biochemistry* **1996**, *35*, 10358−10366.
(49) Wang, G.; Sparrow, J. T.; Cushley, R. J. *Biochemistry* **1997**, *36*, 13657−13666.
(50) Nell, M. J.; Tjabringa, G. S.; Wafelman, A. R.; Verrijk, R.; Hiemstra, P. S.; Drijfhout, J. W.; Grote, J. J. *Peptides*, in press.
(51) Papo, N.; Shai, Y. *Biochemistry* **2004**, *43*, 6393−6403.
(52) Wang, G.; Keifer, P. A.; Peterkofsky, A. *Spectroscopy* **2004**, *18*, 257−264.

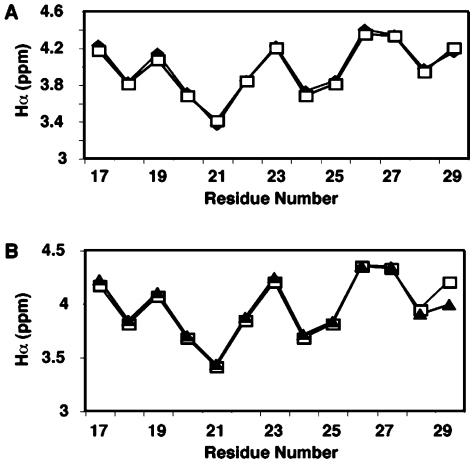


***Figure 2.*** Effects of membrane-mimetic environments (A) and peptide length (B) on the structure of the LL-37 core region. Hα chemical shifts for residues 17−29 measured using LL-37(17−29) in SDS micelles (□ in both A and B), in dioctanoyl phosphatidylglycerol micelles (◆ in A), and measured using LL-37(13−37) in SDS micelles (▲ in B).

***Table 3.*** Structural Statistics of LL-37 Fragments

| peptide region | distance restraints | backbone angles | superimposed region | backbone rmsd (Å) | helical region |
|---|---|---|---|---|---|
| 1−12 | 68 | 10 | 3−7 | 0.29 | 3−7 |
| 13−37 | 165 | 28 | 17−30 | 0.34 | 17−30 |
| 17−29 | 156 | 22 | 18−28 | 0.32 | 18−28 |
| 17−32 | 241 | none | 19−30 | 0.65 | 28−31 |

shifts for the LL-37 core peptide in D8PG and SDS micelles are presented in Figure 2A. The two curves superimposed nicely. Further, there were similar NOE contacts between the hydrophobic side chains of F27 and L28 as well as F17 and V21 in both micelles. These results indicate that the LL-37 core peptide possesses similar structures in the two environments. Near identical structures in these two environments were also found previously for both aurein 1.2[23] and a bacterial membrane anchor.[36] Interestingly, molecular dynamics simulations found that the structure of gramicidin A determined in SDS micelles better represents the structure elucidated in lipid bilayers.[53] All these data would imply that detergent micelles mimic membrane environments well.

Because of the chemical shift similarities of the LL-37 core peptide in SDS and D8PG (Figure 2A), we used deuterated SDS micelles for 3D structure determination of the LL-37 core peptide for the best quality, as deuterated D8PG is not yet commercially available. In total, 156 distance restraints were used in the structural calculations (Table 3). The distance-based structure was refined by natural abundance heteronuclear chemical shifts ($^1H^\alpha$, $^{13}C^\alpha$, $^{13}C^\beta$, and $^{15}N$),[23] because scalar coupling data are difficult to measure for micelle-bound peptides due to line broadening.[21,22] Based on these chemical shifts, peptide backbone angles ($\phi$, $\varphi$) for residues 18−28 were derived from TALOS.[42] Inclusion of these angle restraints led to an excellent Ramachandran plot with 100% of backbone angles of the peptide in the most favored region. Previous studies indicate that, in the absence of angle restraints, such a good geometry may not be obtained especially when the distance restraints are not sufficient.[23] The rmsd for superimposing

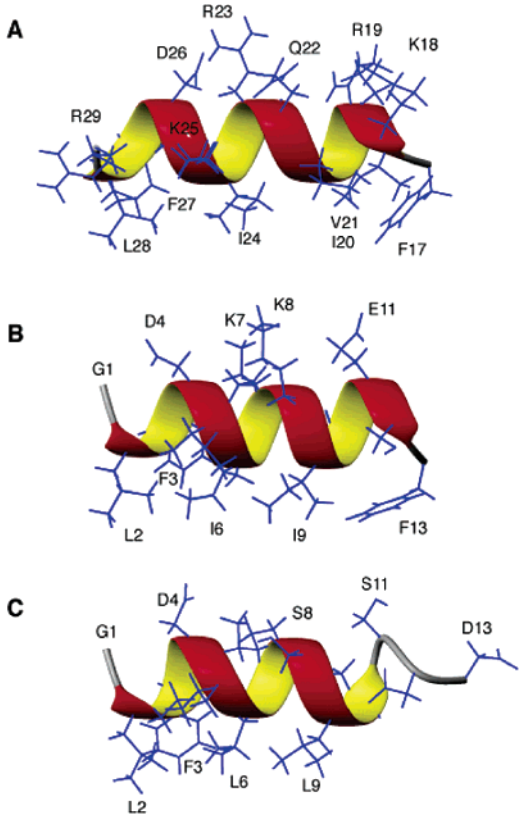


***Figure 3.*** Structure of the LL-37 core peptide (A) and comparison with aurein 1.2 (B)[54] and a bacterial membrane anchor from the N-terminus of glucose-specific enzyme IIA of *E. coli* (C).[63] To facilitate the comparison, the order of the N- and C-end of the LL-37 core peptide is reversed. The Protein Data Bank accession codes for the coordinates of aurein 1.2 and the membrane anchor are 1VM5[23] and 1O53.[36]

backbone atoms of residues 18−28 of the core peptide was 0.32 Å, indicative of a good precision. As shown in Figure 3A, the LL-37 core peptide adopts an amphipathic helical structure. The side chains of residues F17, I20, V21, I24, F27, and L28 are located on the hydrophobic surface, whereas the side chains of residues K18, R19, Q22, R23, D27, and R29 are located on the hydrophilic surface. The amphipathic nature of the structure can also be seen from the potential surface (Figure 4A), where positively and negatively charged side chains are in blue and red, respectively. Such a structural feature is ideal for targeting negatively charged bacterial membranes.

**Comparison of the LL-37 Core Peptide with the Bacterial Membrane Anchor and Aurein 1.2.** The positioning of the two aromatic rings in the structure of the LL-37 core peptide is reminiscent of that observed previously in aurein 1.2 (Table 1), an antimicrobial and anticancer peptide isolated from the Australian Bell Frog.[54] The two aromatic rings in either peptide show contacts with adjacent hydrophobic side chains, forming hydrophobic clusters for membrane binding (Figure 3A and B). In the case of aurein 1.2, an alteration of F13 to isoleucine abolished anticancer activity of the peptide.[54] Alternatively, changing D13 of the nontoxic bacterial membrane anchor (Figure 3C) to F13 converted the nontoxic membrane anchor to an antibacterial peptide.[23] In the case of the LL-37 core peptide, further removal of L28R29 caused a significant reduction in antibacterial activity and a loss in anticancer activity

(53) Allen, T. W.; Andersen, O. S.; Roux, B. *J. Am. Chem. Soc.* **2003**, *125*, 9868−9877.

(54) Rozek, T.; Wegener, K. L.; Bowie, J. H.; Olver, I. N.; Caver, J. A.; Wallace, J. C.; Tyler, M. J. *Eur. J. Biochem.* **2000**, *267*, 5330−5341.

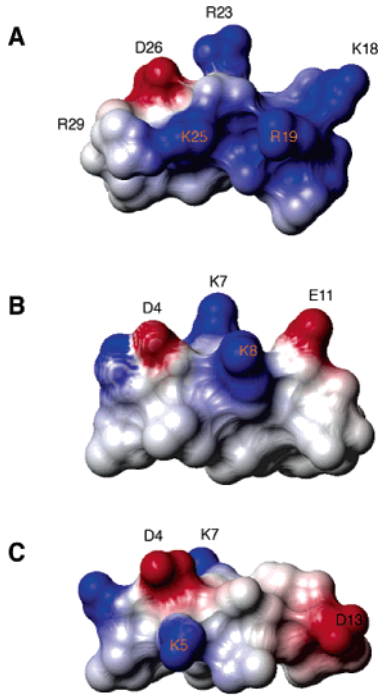


***Figure 4.*** Potential surfaces of the LL-37 core peptide (A), aurein 1.2 from a frog (B), and the bacterial membrane anchor from *E. coli* (C). The figure was made using MOLMOL.[55]

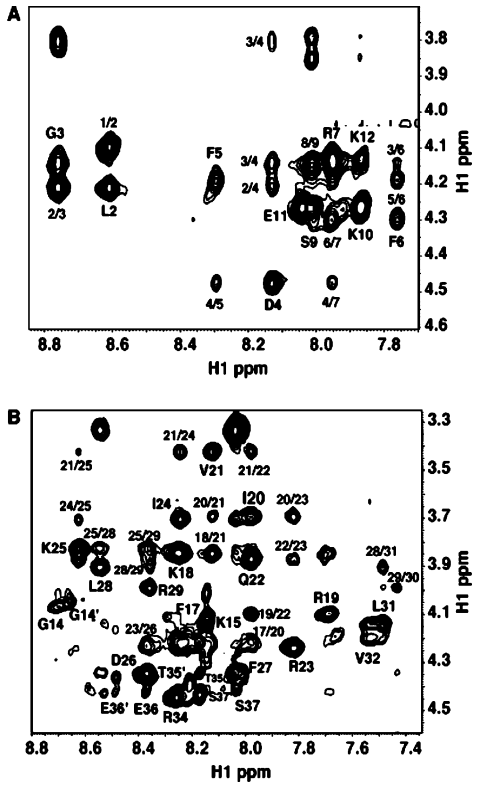


***Figure 5.*** Portions of the NOESY spectra (mixing time 100 ms) of LL-37(1−12) at 15 °C (A) and LL-37(13−37) in SDS micelles at 25 °C, both at pH 5.4. NMR signals were assigned based on the established method.[39] Intraresidue cross-peaks are labeled with the single-letter amino acid code. Interresidue NOE cross-peaks between Hα and amide protons are labeled with arabic numbers. For example, 21/25 stands for the NOE cross-peak from the Hα proton of V21 to the backbone amide proton of K25.

(Table 2). According to the 3D structure in Figure 3A, removal of L28 would disrupt the hydrophobic packing between F27 and L28. All these results indicate the importance of the aromatic-ring-involved hydrophobic clusters for membrane binding.[48]

In terms of inhibiting the growth of *E. coli*, the LL-37 core peptide (MIC 40 $\mu$M) is more active than aurein 1.2 (MIC 75 $\mu$M).[23] Because these two peptides possess the same backbone structure and equivalent hydrophobic clusters (Figure 3), the difference in activity may be determined by the additional number of cationic side chains in the LL-37 fragment. Indeed, there are five cationic side chains in the LL-37 core peptide (K18, R19, R23, K25, and R29) but only two in aurein 1.2 (K7 and K8). In the case of aurein 1.2 and the bacterial membrane anchor, both peptides have two cationic side chains in the membrane-targeting helical domain (Figure 3B and C). The toxic effect of aurein 1.2 on both bacterial and cancer cells[54] was previously ascribed to its broader and longer hydrophobic surface (Figure 4B).[23] In contrast, the absence of cytotoxicity of the bacterial membrane anchor is determined by the short and narrow hydrophobic surface (Figure 4C). The broader hydrophobic surface of aurein 1.2 versus that of the bacterial membrane anchor enabled the former to effectively penetrate into and perturb the bacterial membranes. Thus, increase in either the number of cationic charges or hydrophobicity enhances the cytoxicity of the peptide.

**Structures of the N- and C-Terminal Fragments of LL-37.** Because LL-37 can be cleaved in vivo into similar fragments,[24] we also determined the structures of both LL-37(1−12) and LL-37(13−37) in SDS micelles for a better understanding of the structure−activity relationship. To illustrate the quality of the data, Figure 5 shows a portion of the NOESY spectra for both the N- (A) and C-terminal (B) peptides. As labeled in the spectra of the C-terminal peptide LL-37(13−37), the (i, i + 3) type of NOE cross-peaks covers residues 17−31, indicating a helical structure for that region. The NOE cross-peak from the Hα of V32 to the Hδ of P33 indicates a trans conformation for the proline in LL-37(13−37). As described above, solution structures of the LL-37 fragments were determined based on both distance and angle restraints. In total, 68 and 165 distance restraints were found for the N- and C-terminal fragments, respectively. Based on natural abundance chemical shifts,[23] the backbone angles ($\phi$ and $\varphi$) for residues 3−7 of the N-terminal fragment and residues 17−29 of the C-terminal fragment of LL-37 were restrained in the helical region (Table 3).

According to the MOLMOL analysis,[55] the majority of the structures showed a helical structure in the region corresponding to residues 17−30 (Figure 6A). When the backbone atoms of residues 17−30 were superimposed, the rmsd was 0.34 Å relative to the mean structure. The backbone rmsd increased dramatically to 2.3−2.7 Å, however, when the superimposed region was expanded to include either residues 13−16 or 32−37. An investigation of the NOE list revealed that the number of NOE cross-peaks for those regions was less than 3 per residue, while the average number of NOEs for residues 17−31 was 10. Such an NOE distribution along the polypeptide chain is consistent with the structure in Figure 6A, where the central portion is well defined with both ends "frayed". It is likely that those poorly defined peptide regions do not or weakly interact with the micelles.[36,48]

(55) Koradi, R.; Billeter, M.; Wüthrich, K. *J. Mol. Graphics* **1996**, *14*, 51−55.

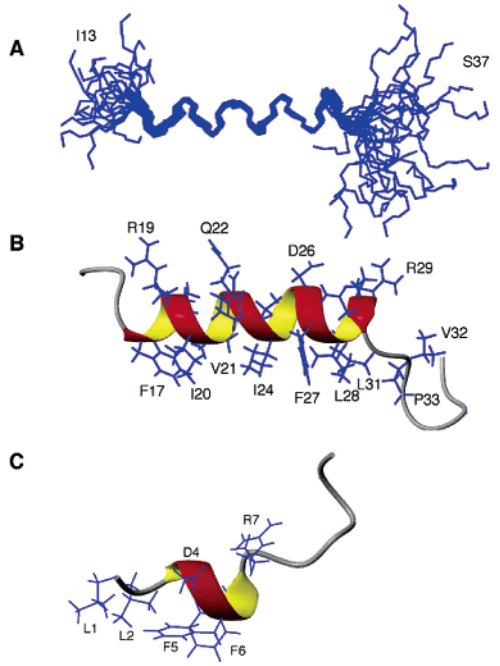


***Figure 6.*** Solution structures of the N- and C-terminal fragments of LL-37 bound to SDS micelles. Structures were determined as described in the Methods section based on both NOE-derived distance restraints and natural abundance chemical shift derived angle restraints.[23] Shown are the backbone (with residues 17−29 superimposed) (A) and ribbon (B) representations of the structure of LL-37(13−37) and a ribbon view of the structure of LL-37(1−12) (C). The aromatic−aromatic interactions between F5 and F6 in LL-37(1−12) are proposed to be essential for LL-37 aggregation.[17,18]

Interestingly, the well-defined helical region in the C-terminal fragment of LL-37 (Figure 6B) corresponds nicely to the LL-37 core peptide (Figure 3A) identified by TOCSY-trim (Figure 1). Thus, a core antimicrobial peptide would also have been found in the C-terminal fragment of LL-37 based on structural determination. Further, TALOS[42] analysis of a set of $^{1}H$, $^{13}C$, and $^{15}N$ chemical shifts of LL-37(13−37) also indicates that residues 17−29 are helical. The agreement of TOCSY-trim with both TALOS analysis and structure determination further supports the usefulness of TOCSY-trim in identifying a core membrane-targeting peptide embedded in a longer sequence. The advantage of TOCSY-trim is that a membrane-binding peptide region could be mapped prior to the completion of 3D structure determination, which usually takes a longer time and more efforts. In our study, LL-37 and its fragments were chemically synthesized at natural abundance and proton-based TOCSY spectra were employed (Figure 1). When LL-37 is isotopically labeled, for example, by using the bacterial system we developed,[44] other NMR techniques such as heteronuclear NOE experiments (small or negative NOEs for flexible regions) and a carbon version TOCSY (strong cross-peaks as in the proton version) could also be applied in identifying minimal membrane-targeting regions.

The antibacterial activity of the LL-37 core peptide is comparable to the longer LL-37 fragments (Table 2). The slightly lower activity of LL-37(13−37) may result from the interference of the disordered regions with membrane binding of the peptide (Figure 6A and B). It also suggests that only cationic and hydrophobic side chains in the membrane-targeting domains contribute to the antibacterial activity of the peptide. In terms of anticancer activity, LL-37(17−29) became slightly less active than the longer ones, indicating that the truncated hydrophobic residues L31 and V32 also play a role in interaction with human cells. The decrease in hydrophobicity of LL-37-(17−29), compared to either LL-37(17−32) or LL-37(13−37), is supported by the slightly shorter retention time on the reversed-phase HPLC column (Table 1).

The structure of the N-terminal peptide LL-37(1−12) is displayed in Figure 6C. Only a one-turn helix covering residues 3−7 was found. The rmsd for superimposing the helical region was 0.29 Å (Table 3). According to the Ramachandran plot, 62%, 18%, 18%, and 2% of the backbone angles for the N-terminal peptide are located in the most favored, additionally allowed, generously allowed, and disallowed regions, respectively. A similar distribution (76%, 15%, 7%, and 2%) was observed for the C-terminal fragment LL-37(13−37). These plots differ from that of the LL-37 core peptide, where 100% of the backbone angles are in the most favored region of the Ramachandran plot. A detailed residue-by-residue analysis found that nearly all residues *not* located in the most favored regions are those in the poorly defined peptide regions, that is, residues 8−12 in the case of LL-37(1−12) and residues 13−16 as well as 31−37 in the case of LL-37(13−37).

In Figure 6C, the aromatic rings of F5 and F6 are perpendicular to each other and packing with the side chain of L2, forming one single hydrophobic cluster. Such an orientation between the aromatic rings of F5 and F6 offers an explanation for the upfield chemical shift of the H$\delta$ protons of F5 at 6.85 ppm (Figure 7A) as a result of the ring current effect of F6. The single hydrophobic cluster in this peptide is responsible for the shortest retention time on the reversed-phase HPLC column (see Table 1). The poor hydrophobicity of the peptide may also be the reason, at least in part, for the lack of antibacterial or anticancer activity. Since aromatic−aromatic interactions play a significant role in stabilizing protein structure,[56] in binding to lipids,[48] and in stabilizing the lipid-free oligomeric structure,[57] we propose that aromatic−aromatic interactions between F5 and F6 are essential for oligomerization of LL-37 observed previously.[17,18]

**Peptide-Aided Signal Assignments of Intact LL-37.** As shown above, the structure of the LL-37 core peptide (Figure 3A) is retained in the C-terminal fragment LL-37(13−37) (Figure 6B) as well. Correspondingly, the H$\alpha$ chemical shift plots for residues 17−29 in the core peptide as well as in LL-37(13−37) against residue number are remarkably similar (Figure 2B). It was tempting to extend this observation to intact LL-37. Unfortunately, it is difficult to achieve a full signal assignment for SDS-bound LL-37 as a consequence of signal overlap in 2D NMR spectra. In the regions where signals were sparse, however, spectral identities between the fragments and intact LL-37 could be seen. The sparse signal regions allowed us to employ the peptide-aided signal assignment approach for partial assignments.[49] For example, the H$\alpha$ of V21 in LL-37 is well resolved. Its chemical shift at 3.40 ppm is identical to those in the LL-37 core peptide (3.41 ppm) and the C-terminal fragment (3.43 ppm). Figure 7A shows the aromatic regions of the NOESY spectra of LL-37(1−12) (panel A), LL-37(13−37) (B), and LL-37 (C). Indeed, the chemical shifts of the H$\delta$ protons of F5 and F6 at 6.85 and 7.31 ppm in the spectrum of

(56) Burley, S. K.; Petsko, G. A. *Science* **1985**, *229*, 23−28.
(57) Wang, G. *FEBS Lett.* **2002**, *529*, 157−161.

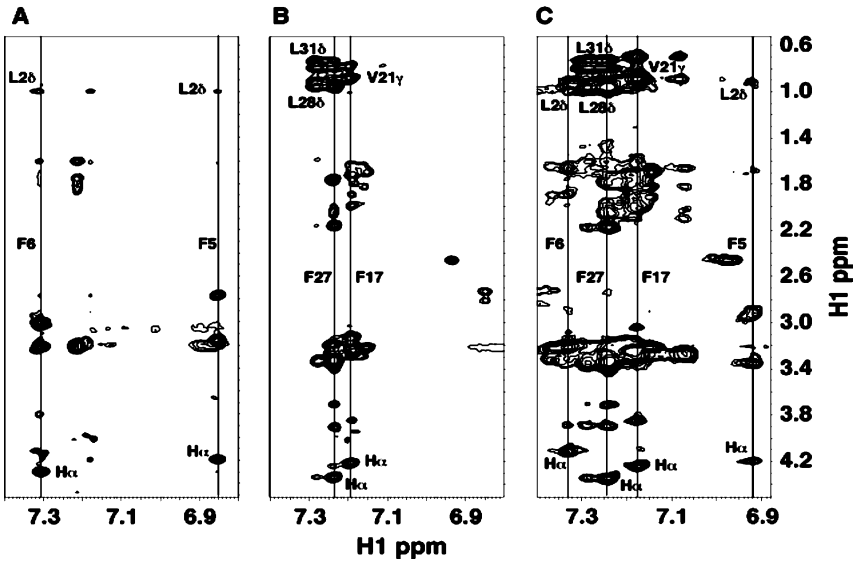


***Figure 7.*** Peptide-aided signal assignments (PASA). Shown are portions of the NOESY spectra of the N-terminal fragment LL-37(1−12) (A), the C-terminal fragment LL-37(13−37) (B), and full-length LL-37 (C) in SDS micelles. Vertical lines indicate the H$\delta$ protons of aromatic residues F5, F6, F17, and F27. Some NOE cross-peaks from the H$\delta$ protons of the aromatic rings to nearby hydrophobic side chains are also labeled. The similar chemical shifts between the fragments and intact LL-37 enabled partial assignments.

LL-37(1−12) are very similar to 6.92 and 7.33 ppm in the spectrum of LL-37. Likewise, the chemical shifts of the H$\delta$ protons of F17 and F27 in the C-terminal fragment (at 7.19 and 7.24 ppm) are nearly identical to those in LL-37 (at 7.18 and 7.24 ppm). Further, there are similar hydrophobic interactions between the aromatic rings and hydrophobic side chains ranging from fragments to intact LL-37 (see Figure 7). Finally, strong TOCSY relays observed for residues 34−37 in LL-37-(13−37) (Figure 1) were also found in intact LL-37. Thus, the structures found in the fragments might also exist in intact LL-37. We may propose a structural model for this important human defense molecule, which consists of two amphipathic helices connected by a yet-to-be-defined linker in the vicinity of G14.

**Structure of a D-Amino Acid Containing Peptide Analogue of LL-37(17−32).** Previous[17,18] and current studies indicate that LL-37 and its fragments showed poor cell selectivity (Table 2). As the only antibacterial cathelicidin peptide in humans, there is high interest in exploiting LL-37 as a template to design novel antimicrobial peptides.[40−42] The toxicity of LL-37-derived peptides to human cells must be abolished. For this purpose, we have exploited the idea of incorporating D-amino acids into the peptide. Shai and colleagues found that incorporation of D-amino acids at every 2−3 residues is effective in disrupting helical structures.[51] Because LL-37(17−32) showed the highest cytotoxic effects on both bacteria and cancer cells (Table 2), it was chosen as a peptide template. Using the Shai's incorporation scheme, we have replaced residues I20, I24, and L28 of LL-37(17−32) by their corresponding D-amino acids. The resultant peptide is referred to as dLL-37(17−32) (Table 1). Antibacterial assays found that this D-amino acid containing peptide retained the same activity as that of LL-37(17−32). Interestingly, dLL-37(17−32) was toxic to neither cancer cells nor normal human cells (Table 2). D-Amino acid incorporation was previously applied to pardaxin,[58] melittin,[59] and other peptides,[60,61] leading to D-peptide analogues with similar antibacterial activities but no cytotoxic effects on mammalian cells. Our study provides another successful example for improving cell selectivity of antimicrobial peptides by D-amino acid incorporation.

To provide insight into the structural basis for the detoxification of the LL-37 peptide by D-amino acid incorporation, we also carried out a structural study of dLL-37(17−32) bound to SDS micelles. The fingerprint region of the NOESY spectrum of this D-amino acid containing peptide is given in Figure 8A. The NOE contacts between adjacent residues, viz., of (i, i + 1) type, are strong, and there are only very few and weak (i, i + 2) or (i, i + 3) types of NOEs and no (i, i + 4) type of NOEs. Such an NOE pattern (e.g., Figure 5B) differs from that observed for the corresponding peptide consisting of all L-amino acids (L-diastereomer), indicating a successful disruption of the canonical $\alpha$ helical structure. Because of a new type of 3D structure, the NOE assignments of dLL-37(17−32) were performed in an iterative manner by starting from those with unique chemical shifts. In total, 241 NOE cross-peaks were used for structural calculation. When TALOS[42] was applied to the analysis of the heteronuclear chemical shifts of the peptide, only residues F27, R29, and N30 were predicted in the helical region. Because of the lack of D-amino acid data in the TALOS program, the results were not included in the structural refinement. A backbone view of the structural ensemble of dLL-37-(17−32) is provided in Figure 8B. The rmsd was 0.65 Å when the backbone atoms of residues 19−30 were superimposed.

At the N-terminus, the structure of dLL-37(17−32) consists of multiple turns, which we refer to as an omega-turn, due to a shape similar to the letter $\omega$ after a 180° flip of Figure 9A. The C-terminal region, residues 28−31, forms a $3_{10}$ helix according to MOLMOL analysis.[55] The aromatic ring of F27 shows hydrophobic contacts to I24, L28, and L31. Similarly, there are interactions from F17 to I20 and V21. These NOE contacts directly bring together the hydrophobic side chains, leading to

(58) Shai, Y.; Oren, Z. *J. Biol. Chem.* **1996**, *271*, 7305−7308.
(59) Oren, Z.; Shai, Y. *Biochemistry* **1996**, *36*, 1826−1835.
(60) Oren, Z.; Ramesh, J.; Avrahami, D.; Suryaprakash, N.; Shai, Y.; Jelinek, R. *Eur. J. Biochem.* **2002**, *269*, 3869−3880.
(61) Chen, Y.; Man, C. T.; Farmer, S. W.; Hancock, R. E. W.; Vasil, M. L.; Hodges, R. S. *J. Biol. Chem.* **2005**, *280*, 12316−12329.

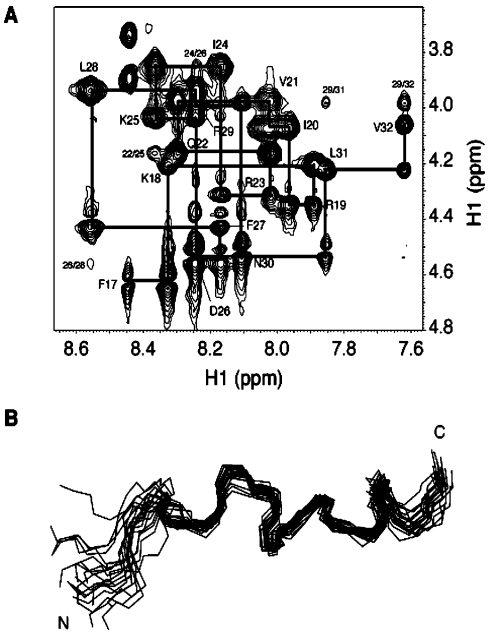


***Figure 8.*** Effects of D-amino acid incorporation on the NMR spectrum and structure of LL-37(17−32). The NOE pattern for the D-peptide (A) is clearly different from that of the L-diastereomer in Figure 5B. Thus, the 3D structure (B), consisting of a twisted omega turn at the N-terminus and a $3_{10}$ helix at the C-terminus, is also different from that shown in Figure 6B, which is entirely helical for the same portion of the peptide. In (A), the phases of the cross-peaks of F17, D26, F27, and N30 in the vicinity of water were influenced by a water flipback pulse.

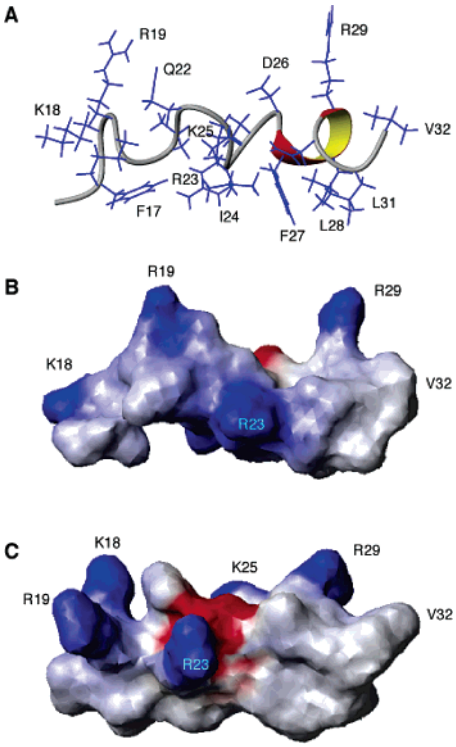


***Figure 9.*** Structural basis of detoxification of LL-37(17−32) by introducing D-amino acids. Although the D-peptide retains an amphipathic structure (A) and identical toxic effects on bacteria (Table 2), the hydrophobic defect in the D-peptide elucidated by structural determination (B) caused the loss of toxic effects on human cells. Similar hydrophobic defects do not occur in the structure of the corresponding L-diastereromer (C).

a new amphipathic structure with a distorted backbone structure (Figure 9A).

Because both dLL-37(17−32) (Figure 9B) and LL-37(17−32) (Figure 9C) adopt an amphipathic structure with five positively charged side chains on the hydrophilic surface, they should possess an identical positive membrane perturbation potential when attacking the negatively charged bacterial membranes in terms of electrostatic interactions. The identical antibacterial activity of the D- and L-form peptides suggest that electrostatic interactions dominate. The hydrophobic part, however, may have determined their toxic differences to human cells (Table 2). One of the current approaches for quantifying the hydrophobicity of peptides is to use the retention time on a reversed-phase HPLC.[61,62] The retention times of LL-37(17−32) and dLL-37(17−32) are 42 and 29.8 min, respectively, indicating that the latter is much less hydrophobic than the former. Structurally, a clear defect (under residue R19 in Figure 9B) could be seen on the hydrophobic surface of dLL-37(17−32). This was caused primarily by the deviations of I20 and V21 from the hydrophobic surface. In other words, the distortion of the peptide backbone conformation by D-amino acids caused an out-of-phase packing between the two hydrophobic clusters involving aromatic phenylalanines (Figure 9A). As a comparison, the hydrophobic side chains in the structure of the same peptide region, consisting of L-amino acids, all pack in-phase to form a single *coherent* hydrophobic surface (Figures 6B and 9C). We propose that the hydrophobic defects in Figure 9B provide a structural basis for the poor hydrophobicity of this D-amino acid containing peptide.

To provide additional insight into the basis for cell selectivity, we also compared dLL-37(17−32) with the bacterial membrane anchor.[63] Because the nontoxic bacterial membrane anchor (Figures 2C and 3C) interacts with anionic lipids but not with zwitterionic lipids, it is proposed that its hydrophobic surface contains the minimal requirement for bacterial membrane targeting.[23,63] The retention time of the bacterial membrane anchor was found to be 29.5 min, which is essentially identical to that of dLL-37(17−32) (Table 1). In analog to the bacterial membrane anchor, one would predict that dLL-37(17−32) does not bind to the membranes of human cells rich in zwitterionic lipids. This would appear to be the case as dLL-37(17−32) lost its toxicity to human brain endothelial cells as well as cancer cells (Table 2). Because a reduced hydrophobicity after introducing D-amino acids was also observed for other peptides,[61,64] it may be the case that the incoherent hydrophobic packing offers a useful interpretation at the structural level for D-amino acid detoxification.

## Conclusion

In this study, LL-37 was dissected into fragments (Table 1) to understand the structure−activity relationship. A short helix was found in the N-terminal fragment, LL-37(1−12). This single hydrophobic cluster in the N-terminal peptide is not toxic to either bacteria or cancer cells (Table 2). In contrast, the C-terminal fragment, LL-37(13−37), kills both bacteria and cancer cells. The solution structure of LL-37(13−37) contains a well-defined central helix with both ends "frayed" (Figure 6). This central amphipathic helix is responsible for the antibacterial and anticancer activity of LL-37, because the

(62) Kim, S.; Kim, S. S.; Lee, B. J. *Peptides* **2005**, *26*, 2050−2056.
(63) Wang, G.; Peterkofsky, A.; Clore, G. M. *J. Biol. Chem.* **2000**, *275*, 39811−39814.
(64) Rosenfeld, Y.; Papo, N.; Shai, Y. *J. Biol. Chem.* **2005**, *281*, 1636−1643.

disordered regions at both ends can be deleted with little influence on the antibacterial activity of the peptide. This structured central region of LL-37 (also supported by TALOS analysis) corresponds well to the shortest LL-37 core antibacterial peptide identified by TOCSY-trim (Figure 1 and the artwork for the Table of Contents). Thus, TOCSY-trim proves to be a useful technique for efficient identification of a core membrane-targeting antimicrobial peptide hidden in a longer polypeptide sequence prior to the completion of structural determination. Because only a few peptides (Table 1) were synthesized, TOCSY-trim is cost-effective in trimming of nonessential membrane-targeting regions from long peptides.

The structural similarities (Figures 3 and 4), ranging from the bacterial membrane anchor discovered in *E. coli* glucose-specific enzyme IIA[63] to aurein 1.2 isolated from the Australian Bell Frog *Lithoria aurea*,[54] and to the LL-37 core peptide identified from the only human cathelicidin (this study), allow us to better understand the antibacterial activity of LL-37. Due to the equivalent hydrophobic surfaces, higher antibacterial activity of the LL-37 core peptide (Figure 3A) than that of aurein 1.2 (Figure 3B) is attributed to additional cationic side chains in the former (5 vs 2), which prefer negatively charged bacterial membranes. In contrast, the higher activity of aurein 1.2 than that of the bacterial membrane anchor (inactive) was determined by a higher hydrophobicity of the former than that of the latter (Table 1), since both peptides have two cationic lysines in the membrane-binding helical domains.

Incorporation of D-amino acids could diminish the cytotoxicity of the LL-37 peptides without sacrificing its toxic effect on bacteria. Therefore, it is feasible to design selective antibacterial peptides using human LL-37 as a template. We have elucidated the structural basis for this detoxification. D-Amino acids disrupted the canonical helical structure[65] by distorting the peptide backbone (Figure 9A). The out-of-phase packing of the two aromatic-residue-involved hydrophobic clusters caused hydrophobic defects in the amphipathic structure of dLL-37(17−32), leading to a poor hydrophobicity (Table 1) and rendering it insufficient for targeting human cells (Table 2). It is noteworthy that the poor hydrophobicity of the bacterial membrane anchor is due to a short amphipathic helix (Figure 3C) as well as a narrow hydrophobic surface (Figure 4C). In conclusion, reduction in peptide hydrophobicity could be a fundamental approach for improving cell selectivity of antimicrobial peptides, whether it is achieved by decreasing the content of hydrophobic residues (Figure 3C) or by D-amino acid incorporation (Figure 9A). This unified concept for improving peptide selectivity by tuning hydrophobicity is useful for designing potent antimicrobial peptides that substitute traditional drug-resistant antibiotics.

**Acknowledgment.** This work was supported by the Startup Fund from University of Nebraska Medical Center, Nebraska EPSCoR, Nebraska Health and Human Services System (G.W.), and, in part, NIH Grant R01-CA93558 (D.W.M.). The authors thank Paul Keifer for maintaining the 600-MHz NMR spectrometer and Dan Garrett, Frank Delaglio, John Kuszewski, and Charles Schwieters (NIH) for NMR software.

**Supporting Information Available:** A full list of all authors for ref 3 is provided. This material is available free of charge via the Internet at http://pubs.acs.org.

JA0584875

(65) Mitchell, J. B. O.; Smith, J. *Proteins* **2003**, *50*, 563−571.
(66) Waddell, W. J. *J. Lab. Clin. Med.* **1956**, *48*, 311−314.